Classical Density Functional Theory for Methane Adsorption in Metal-Organic Framework Materials

Jia Fu, Yun Tian, and Jianzhong Wu
Dept. of Chemical and Environmental Engineering, University of California, Riverside, CA 92521

DOI 10.1002/aic.14877
Published online July 2, 2015 in Wiley Online Library (wileyonlinelibrary.com)

Natural gas is considered as a promising alternative to petroleum as the next generation of primary transportation fuel owing to relatively smaller carbon footprint and lower SO_x/NO_x emissions and to fast developments of shale gas in recent years. Since the volumetric energy density of methane amounts to only about 1% of that of gasoline at ambient conditions, natural gas storage represents one of the key challenges for prevalent deployment of natural gas vehicles. In this work, we present a molecular thermodynamic model potentially useful for high-throughput screening of nanoporous materials for natural gas storage. We investigate methane adsorption in a large library of metal-organic frameworks (MOFs) using four versions of classical density functional theory (DFT) and calibrate the theoretical predictions with extensive simulation data for total gas uptake and delivery capacity. In combination with an extended excess entropy scaling method, the classical DFT is also used to predict the self-diffusion coefficients of the confined gas in several top-ranked MOFs. The molecular thermodynamic model has been used to identify promising MOF materials and possible variations of operation parameters to meet the Advanced Research Projects Agency-Energy (ARPA-E) target set by the U.S. Department of Energy for natural gas storage. © 2015 The Authors AIChE Journal published by Wiley Periodicals, Inc. on behalf of American Institute of Chemical Engineers *AIChE J*, 61: 3012–3021, 2015
Keywords: multiscale modeling, classical density functional theory, excess entropy scaling, methane storage, metal organic frameworks

Introduction

Adsorption thermodynamics plays a pivotal role in traditional as well as modern chemical engineering ranging from separation processes and heterogeneous catalysis to various experimental tools for chemical analyses such as chromatography.[1,2] From a practical point of view, one of the most useful thermodynamic models for gas adsorption was established by Myers and Prausnitz, published in the *AIChE Journal* about 50 years ago.[3] We are pleased to dedicate this article to the special issue honoring Professor John Prausnitz.

According to conventional wisdom, adsorption is an interfacial phenomenon related to adhesion of molecules, atoms, or ions at a surface. Whereas in classical thermodynamics concepts such as surface area and binding energy are indispensable to describe the interfacial phenomenon, Myers and Prausnitz took a radically different approach by extending the ideal solution model for vapor-liquid equilibria to adsorption of gas mixtures. The "solution model" is remarkably accurate for predicting the adsorption isotherm of a gas mixture from those for pure components at moderate pressure, yet it is computationally convenient for practical applications. Because the number of pure species is limited in comparison to that for mixtures, the solution model has been invaluable for design and optimization of industrial adsorption processes and remains relevant today.[4]

Driven by increasing concerns over global climate change and rapid developments in renewable energy, research in gas adsorption has seen considerable growth in recent years. However, the main focus of current literature has been shifted from adsorption equilibria *per se* to discovery of novel nanoporous materials, in particular open-framework materials promising for large-scale hydrogen/methane storage or for selective adsorption of carbon dioxide from gas mixtures.[5] Unlike conventional adsorbents such as activated carbon or silica gel, open-framework materials are porous crystalline solids viable for solution synthesis by coordinate bonding of secondary building units (SBUs), that is, organic linkers and organometallic/nonmetallic nodes that can sel-organize into periodic and porous frameworks.[6] Theoretical investigations are useful to acquire a better knowledge of adsorbate-adsorbent interactions and, perhaps more important, for discovery and rational design of nanoporous materials tailored to specific adsorbates. The modular nature of the building blocks makes the framework structures predictable based on the topology and the geometry of specific link-node coordination complexes, rendering unprecedented opportunities for computational design/discovery of crystalline porous materials, and to have a precise

Additional Supporting Information may be found in the online version of this article.

Correspondence concerning this article should be addressed to J. Wu at jwu@engr.ucr.edu

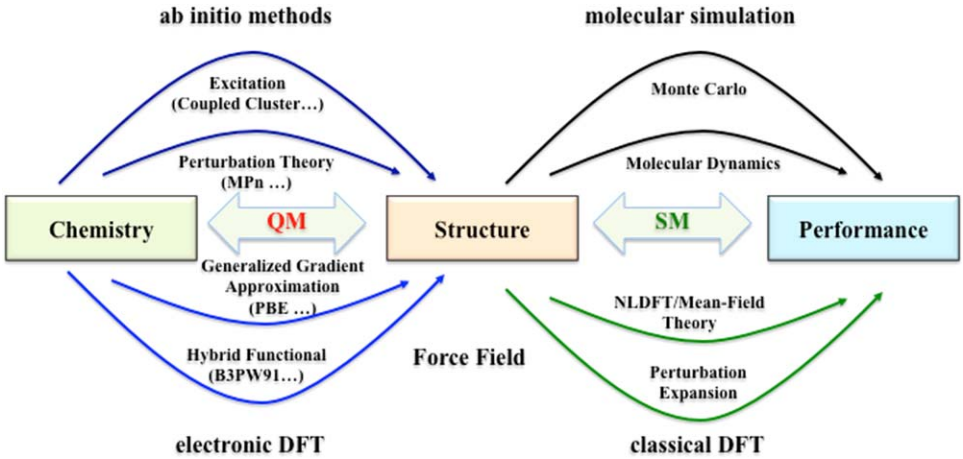

Figure 1. Computational materials design involves quantum mechanical (QM) calculations for understanding the chemistry of individual building blocks and the microscopic structure for molecules and solids, and statistical-mechanical (SM) calculations to predict their performance under diverse thermodynamic conditions.

Because multiple approaches are available for both QM and SM calculations, practical procedures for multiscale modeling should be calibrated with extensive experimental data in terms of both theoretical accuracy and computational efficiency. [Color figure can be viewed in the online issue, which is available at wileyonlinelibrary.com.]

control over their porosity and atomic compositions (size, shape, and functionality). Molecular modeling can help to identify specific open-framework materials from a virtually infinite number of SBU combinations to meet specific practical needs.[7–10]

Whereas there have been impressive theoretical developments toward the discovery of better adsorbents for gas storage and separation,[11–14] computational materials design remains in early development; there are enormous challenges from practical perspectives. To predict material performance from the chemistry of its building blocks, we need efficient multiscale modeling methods that account for not only intrinsic properties in a vacuum but also interactions with a working environment under diverse thermodynamic conditions. As illustrated schematically in Figure 1, computational materials design (or discovery) entails quantum mechanical (QM) calculations for determining electronic properties as well as molecular and crystal structures, and statistical mechanical (SM) calculations for predicting the physicochemical properties of materials under different environments. Myriad computational methods are available for predicting electronic, molecular, and thermodynamic properties.[15] Typically, these computational methods are established in the context of drastically different theoretical frameworks; approximations are inevitable at each level. As a result, multiscale modeling requires a judicious selection of QM and SM methods. An optimal choice resides not necessarily only in terms of the theoretical rigor at individual scales but, perhaps more important, a reliable connection between different methods and the overall computational efficiency to attain pragmatic goals.

Amid numerous computational tools in QM and SM, density functional theory (DFT) provides a unified mathematical framework to describe the properties of many-body systems using the one-body density profiles as the fundamental variables. Whereas the original concepts, as first introduced many years ago by Hohenberg and Kohn,[16] were intended to provide an alternative to the Schrödinger equation for predicting ground-state electronic properties, the mathematical framework has been generalized, applicable to electronic systems at finite temperature and to statistical-mechanical systems including those containing classical particles and polymers.[17] Nowadays DFT is best known for its applications to electronic systems, due to its extreme popularity in computational chemistry and materials science.[18] However, the practicality of classical DFT for studying adsorption and other interfacial phenomena has been well established.[19] For example, classical DFT programs have been routinely used to analyze experimental data for characterization of porous materials by gas adsorption.[20] Because DFT calculations avoid explicit multibody wave functions for quantum systems or microstates for thermodynamic systems containing classical particles, its computational efficiency is by far superior to wave-function-based QM methods and conventional molecular simulations. The computational efficiency and flexibility in formulation of density functional make DFT an ideal choice for multiscale modeling for both QM and SM calculations.[21]

In a previous work,[22] we demonstrated that the classical DFT could be used for rapid screening a large library of metal-organic frameworks (MOFs) potentially useful for H_2 storage. Using extensive Monte Carlo simulation data as the benchmark, we tested the theoretical performance of four versions of free-energy functionals that are commonly used in the literature to describe the thermodynamic properties of inhomogeneous fluids.[23–26] All these functionals incorporate the modified fundamental measure theory (MFMT)[27] to account for molecular excluded-volume effects but they differ in representing the attraction part of the excess free energy. In stark contrast to previous calibrations with model systems containing Lennard-Jones (LJ) fluids in idealized pores, we find that the theoretical predictions are sensitive to specific gas components (e.g., N_2 adsorption vs. hydrogen storage) and thermodynamic conditions. In this work, we test the performance of different classical DFT methods for predicting methane adsorption in model slit pores as well as in a large library of hypothetical nanostructured materials. In addition to adsorption isotherms, we consider methane diffusivity in top-performance MOFs using an extended excess-entropy scaling scheme proposed in our earlier work.[28] After extensive calibration with our simulation results, the DFT methods have been applied to identify promising MOF materials for methane

storage and possible variations of operation conditions to attain the adsorption target set by the U.S. Department of Energy (DOE) for natural gas storage in transportation vehicles.

Molecular Model and Theory

The theoretical models for predicting adsorption isotherms and diffusivity have been reported in our previous publications.[22,28] For completeness, here we recapitulate only the basic ideas of classical DFT and the computational procedures. In Supporting Information, we present the key equations from the four versions of the excess free energy functional used in this work and additional results from classical DFT predictions.

Molecular model

To describe gas adsorption in MOF materials, we need to define both bonded and nonbonded interactions among MOF atoms, and MOF-gas and gas-gas pair interactions in addition to temperature T and pressure P of the gas phase. As in our previous work, we assume that the MOF materials are sufficiently rigid so that their crystalline structures are unchanged by gas adsorption. The crystallographic information files of MOF materials are adopted from the hypothetical library constructed by Wilmer et al.[11]

As a general rule for selecting the size of the computation box, we use a $2 \times 2 \times 2$ supercell of the crystalline structure for each material. The conventional periodic boundary conditions are applied to all directions. For most MOFs considered in this work, the $2 \times 2 \times 2$ supercell ensures that each dimension of the simulation box is larger than twice of the cutoff distance (1.29 nm). For MOFs with very small unit cells, however, we increase the supercell size by adding more repeating unit cells of the crystalline structure such that each dimension is larger than twice of the cutoff distance. As usual, methane molecules are represented by LJ particles, with parameters, ε_{CH4}/k_B=148.0 K and σ_{CH4}=3.73 Å, obtained from the TraPPE force field.[29] For each gas molecule inside the MOF material, the potential energy at position $\mathbf{r}$ is approximated by pairwise-additive interactions with all solid atoms

$$V^{\text{ext}}(\mathbf{r}) = \sum_{i \in \text{MOF}} u_{if}(\mathbf{r}-\mathbf{r}_i) \tag{1}$$

where subscript i represents the ith atom from the MOF framework, and $\mathbf{r}_i$ stands for the position of atom i. The pair potential between atom i and gas molecule f, $u_{if}(\mathbf{r})$, is also represented by the LJ potential

$$u_{if}(r) = 4\varepsilon_{if}\left[\left(\frac{\sigma_{if}}{r}\right)^{12} - \left(\frac{\sigma_{if}}{r}\right)^{6}\right] \tag{2}$$

where parameters ε_{if} and σ_{if} are calculated from the Lorentz-Berthelot (LB) mixing rule. In both simulations and classical DFT calculations performed in this work, the LJ parameters for the MOF atoms are taken from the universal force field.[30]

Adsorption thermodynamics

Classical DFT allows us to predict the local number density of gas molecules within the adsorbent phase, viz., inside each MOF material[31]

$$\rho(\mathbf{r}) = \rho_b \exp[-\beta V^{\text{ext}}(\mathbf{r}) - \beta\Delta\mu^{\text{ex}}(\mathbf{r})] \tag{3}$$

where ρ_b stands for the number density of gas molecules in the bulk, $\beta = 1/(k_B T)$, and k_B is the Boltzmann constant. The last term on the right hand side of Eq. 3 $\Delta\mu^{\text{ex}}(\mathbf{r}) = \mu^{\text{ex}}(\mathbf{r}) - \mu_b^{\text{ex}}$ represents the deviation of local excess chemical potential $\mu^{\text{ex}}(\mathbf{r})$ from that corresponding to the bulk phase, μ_b^{ex}. Thermodynamic properties of the gas phase, including ρ_b and μ_b^{ex} as functions of T and P, are calculated from the modified Benedict-Webb-Rubin equation of state.[32] In general, the local chemical potential depends on the local density profile $\rho(\mathbf{r})$; it must be determined self-consistently from Eq. 3 by iterations.

Intuitively, Eq. 3 may be understood as the Boltzmann distribution of gas molecules in the presence of an external field, $V^{\text{ext}}(\mathbf{r})$. Within the framework of classical DFT, this equation is formally exact. Approximations are introduced only in calculating the local excess chemical potential; this quantity can be derived from the functional derivative of the excess Helmholtz energy, $F^{\text{ex}}(\mathbf{r})$

$$\mu^{\text{ex}}(\mathbf{r}) = \delta F^{\text{ex}}(\mathbf{r})/\delta\rho(\mathbf{r}). \tag{4}$$

Like the excess properties of a uniform thermodynamic system, $F^{\text{ex}}(\mathbf{r})$ accounts for the thermodynamic nonideality due to intermolecular interactions. The excess Helmholtz energy is an intrinsic property independent on the external potential, that is, interaction of gas molecules with the adsorbent atoms. If the intermolecular interaction between gas molecules is negligible, the excess Helmholtz energy vanishes. In that case, Eq. 3 corresponds to the distribution of ideal-gas molecules inside the porous material.

Whereas accurate expressions have been developed for $F^{\text{ex}}(\mathbf{r})$ of inhomogeneous simple fluids below the vapor-liquid critical temperature,[23,33] little is known about their performance at high temperature and pressure, that is, conditions relevant to gas adsorption in typical industrial processes. In this work, we consider four versions of classical DFT that have been used predicting hydrogen adsorption in various MOF materials. All these functionals are based on the modified fundamental measure theory (MFMT)[27] to describe molecular excluded volume effects but differ in contribution to account for intermolecular attractions. The attractive part of the excess Helmholtz energy functional is distinguished in terms of the mean-field approximation (MFA),[24] the first-order mean-spherical approximation (FMSA),[23] and two slightly different forms of weighted density approximations (WDA-Y[25] and WDA-L[26]). The equations for these functionals and numerical details are discussed in Supporting Information.

Total gas adsorption is conventionally expressed as the volume of adsorbed gas molecules per unit volume of the porous material at the standard state (STP). Total adsorption Γ can be calculated from the molecular density profile by integration over the supercell

$$\Gamma = \frac{k_B T_0}{P_0 V}\int \rho(\mathbf{r})\mathrm{d}\mathbf{r} \tag{5}$$

where $P_0 = 1$ atm, $T_0 = 25^\circ$C, and V is the supercell volume. For applications to gas storage, we are mostly interested in the delivery amount, Γ_{del}, that corresponds to the change in total gas uptake by the material at compression and release conditions. Total gas adsorption or delivery amount should not be confused with the surface excess Γ^{ex} conventionally defined as

$$\Gamma^{\text{ex}} = \frac{k_B T_0}{P_0 V}\int [\rho(\mathbf{r}) - \rho_b]\mathrm{d}\mathbf{r} \tag{6}$$

In general, the local number density of gas molecules inside a nanostructured material is highly inhomogeneous due to extreme confinement and attraction from adsorbent atoms.

The difference between absolute and excess adsorption is negligible only when the pressure of the bulk gas is sufficiently low.

Given an expression for the excess Helmholtz energy functional, we can derive the excess entropy of gas molecules inside the porous material from the thermodynamic relation

$$S^{\mathrm{ex}} = -\left(\frac{\partial F^{\mathrm{ex}}}{\partial T}\right)_{\beta\mu,V} \tag{7}$$

and the heat of adsorption from

$$Q = -T\left(\frac{\partial \Delta\Omega}{\partial T}\right)_{\beta\mu,V} \tag{8}$$

In Eq. 8, $\Delta\Omega$ represents the difference between the grand potential of gas molecules in the porous material and that of the same amount of the bulk gas at the same temperature and chemical potential

$$\Delta\Omega = k_{\mathrm{B}}T\int d\mathbf{r}\rho(\mathbf{r})\{\ln[\rho(\mathbf{r})/\rho_{\mathrm{b}}]-1-\beta\mu_{\mathrm{b}}^{\mathrm{ex}}+Z+\beta V_{\mathrm{ext}}(\mathbf{r})\}+F^{\mathrm{ex}}[\rho(\mathbf{r})] \tag{9}$$

where $Z = Z(T,P)$ stands for the compressibility factor of the bulk gas. While adsorption is not explicitly studied in this work, we note that gas pressure inside a porous material corresponds to a second-order tensor where each element varies with the position. As a result, the adsorbed gas does not have an enthalpy as typically defined in classical thermodynamics for bulk fluids. Confusion might arise if one calculates the of adsorption based on enthalpy changes. In writing Eq. 8, we assume that the porous material is rigid such that gas adsorption has negligible effect on the solid's entropy.

Excess entropy scaling for calculating gas diffusivity

As in our previous work,[28] we assume that self-diffusivity of gas molecules in a porous medium, here designated as D_{s}, may be determined from a linear combination of those predicted from the Knudsen diffusion model and the excess-entropy scaling method

$$\ln D_{\mathrm{s}} = \left(1-\frac{\alpha\sigma^3}{v_{\mathrm{free}}}\right)\ln D_K + \frac{\alpha\sigma^3}{v_{\mathrm{free}}}\ln D_{\mathrm{E}} \tag{10}$$

where v_{free} represents the total accessible volume of the porous material divided by the number of confined gas molecules,[34] α is a constant reflecting the maximum molecular packing density, and σ is the LJ diameter for the gas molecules. In Eq. 10, $\alpha\sigma^3/v_{\mathrm{free}}$ may be interpreted as the fraction of the free space inside the pore occupied by gas molecules. In the limit of closest packing, we may estimate α from that for spherical particles in a face-centered-cubic lattice

$$\alpha_{\mathrm{FCC}} = \sqrt{2}/2 \tag{11}$$

Equation 11 provides a first-order estimate for α if no additional information is available. For best agreement with simulation or experimental data, however, α may be used as an adjustable parameter. While this parameter varies slightly for different systems depending on crystal structure, it is independent of the thermodynamic conditions of the bulk gas including temperature and pressure.

The Knudsen model applies to gas diffusion at infinite dilution

$$D_{\mathrm{K}} = \lim_{\rho_b\to 0} D_{\mathrm{s}} \tag{12}$$

where the limiting value can be obtained from performing MD simulation at low gas pressure. Excess-entropy scaling accounts for contributions due to gas-gas interactions inside the pore, estimated from Rosenfeld's scaling rule[35]

$$D_{\mathrm{E}} = \frac{0.585}{\rho_{\mathrm{av}}^{1/3}}\sqrt{\frac{k_{\mathrm{B}}T}{m}}\exp(0.788S^{\mathrm{ex}}/Nk_{\mathrm{B}}) \tag{13}$$

where m represents the molecular mass, ρ_{av} is the average number density of gas molecules inside the porous material, and N represents the total number of adsorbed gas molecules. With the excess entropy calculated from classical DFT, the hybrid method provides an efficient procedure to predict the self-diffusion coefficient of gas molecules in nanoporous materials as a function of temperature and bulk pressure.[28]

Results and Discussion

Adsorption in slit pores

The four classical DFT methods considered in this work have been calibrated in previous publications by extensive comparison with simulation data for inhomogeneous LJ fluids in model systems near a planar wall or in slit pores. At conditions near vapor-liquid equilibrium, the MFA fails to reproduce the depletion of a LJ fluid near a hard or weakly attractive surface, while the FMSA performs rather well in comparison with simulation.[23,33] Surprisingly, all free-energy functionals including MFA are highly accurate for predicting the adsorption of LJ fluids in slit pores. Regrettably, previous publications were mostly focused on comparisons for model systems at low temperatures (<200 K) that have little relevance to practical methane storage.

In this work, the classical DFT methods are first tested with simulation results for methane adsorption in slit pores of different widths and surface energies at room temperature (298 K). Figure 2 shows theoretical predictions for total adsorption and comparison with simulation data. FMSA overestimates total adsorption if the surface is weakly attractive, while the opposite holds for MFA predictions. Conversely, both weight-density approximations (WDA-L and WDA-Y) agree very well with simulation data at all conditions (Figure 2a). For adsorption in slit pores with more attractive walls (Figure 2b), the three versions of non-mean-field methods give virtually identical results. However, MFA underestimates total adsorption compared to simulation data. The poor performance of MFA is somewhat anticipated because it neglects correlation effects due to van der Waals attractions. Because correlation effects contribute to a negative chemical potential, consideration of the correlation contribution would increase total adsorption.

Adsorption and delivery capacities

The performance of different DFT methods for methane adsorption in porous materials may not be fully consistent with that for simple systems. To illustrate, we consider methane adsorption in two representative MOF materials, MOF-5[36] and Cu-BTC,[37] at room temperature. Figure 3 compares total adsorption predicted from different classical DFT methods with results from Grand Canonical Monte Carlo (GCMC) simulation. Overall, the four versions of classical DFT methods all show good agreement with simulation data. However, their

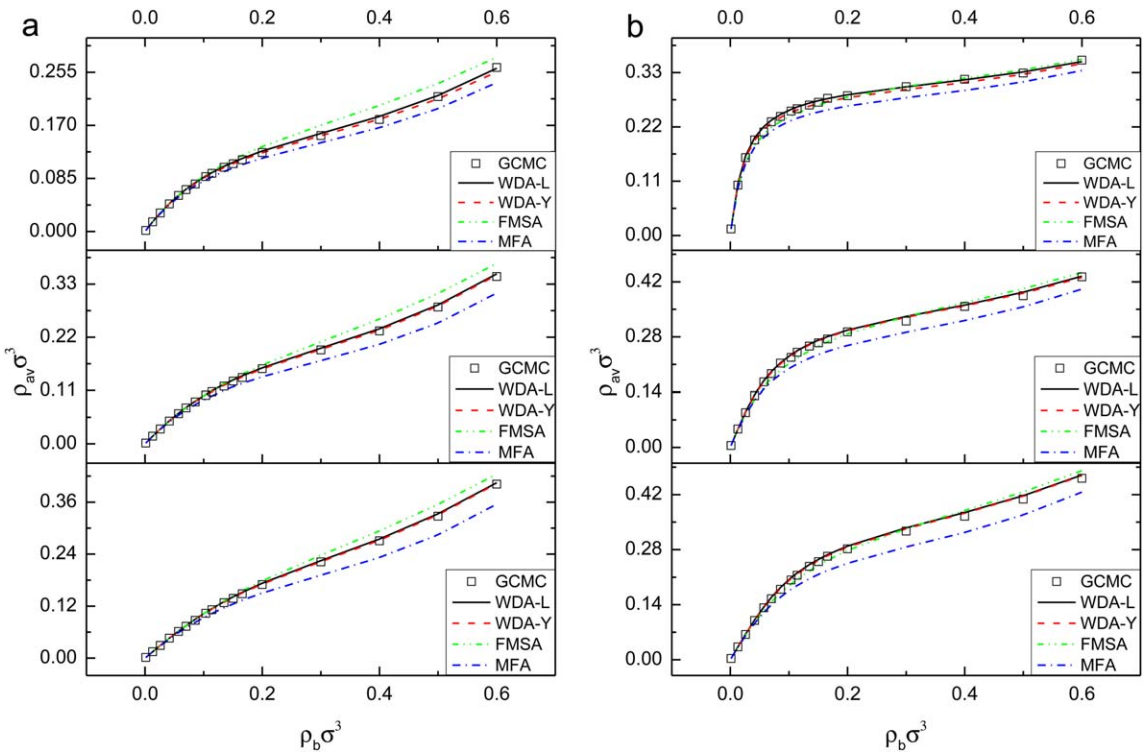

Figure 2. a) Average density (ρ_{av}) in slit pores of reduced width H/σ = 2, 3, 4 from top to bottom at 298K. The interaction between the gas molecule and each wall is described with Steele's 10-4-3 potential, where $\sigma_{sf} = \sigma$, $\varepsilon_{sf} = 0.5\varepsilon$, and $\Delta = 0.7071\sigma$; b) The same as (a) except $\varepsilon_{sf} = \varepsilon$.

[Color figure can be viewed in the online issue, which is available at wileyonlinelibrary.com.]

accuracies are slightly different for different materials. In stark contrast to their performance in slit pores, MFA and FMSA are more accurate than WDA-L and WDA-Y for gas adsorption in MOF-5 at room temperature over the entire range of testing pressures. Both WDA methods overestimate total adsorption especially at intermediate pressures. For methane adsorption in Cu-BTC, however, WDA-Y reproduces GCMC data very well. While WDA-L and FMSA slightly underestimate the storage capacity at moderate pressures, total adsorption predicted by MFA is noticeably smaller than those from other DFT methods at high gas loadings. As indicated in our previous study,[22] the performance of classical DFT methods for gas adsorption in nanoporous materials depends also on testing conditions.

For potential applications to material discovery, the classical DFT methods should be calibrated in the context of multiscale modeling and benchmarked with a large set of experimental data. While novel computational methods for predicting the crystal structures of framework materials and their interactions with gas molecules are rapid emerging,[38] much work remains for systematic calibration of multiscale modeling methods. In this work, we confine our interest to comparing theoretical predictions with GCMC data for methane adsorption in over 1000 MOF materials at various thermodynamic conditions. The crystal structures of these materials are from the Northwestern hypothetic MOF database,[11] generated according to the topology of some common SBUs. These materials have been studied before for methane storage using GCMC simulations[11] and thus provide a good basis to test the performance of different classical DFT methods for materials screening. For validation of the theoretical performance, we consider only 1200 materials from the MOF database, that is, top 300 with the largest excess CH_4 adsorption in weight; top 300 with the largest excess CH_4 adsorption in volume; top 300 with the largest void fraction; top 300 with the largest surface area (m^2/cm^3), all evaluated at 298 K and 35 bar. We believe that these materials are most important for studying methane adsorption and provide a good benchmark for calibration of the four classical DFT methods considered in this work.

Figure 4 shows theoretical results predicted by MFA in comparison with GCMC data. Similar comparisons for other classical DFT methods are presented in Supplementary Materials. In addition to total adsorption at 298 K, we consider also methane delivery for each material when the pressure is reduced from 35 bar to 5 bar at the same temperature. The thermodynamic conditions for the bulk gas are in line with the ARPA-E target for methane storage. Table 1 summarizes the root-mean-square deviations (RMSD) and theory-simulation correlation coefficients (the R values) for different classical DFT methods. In general, all four classical DFT methods show good agreements with the GCMC data for total methane adsorption at the ARPA-E target condition. Surprisingly, MFA gives the best results when compared with simulation data, with RMSD = 7.90 cm^3(STP)/cm^3 and $R^2 = 0.99$. This functional is mathematically simpler than FMSA and weighted-density approximations; it is also numerically more stable and easier to converge in solving for the molecular density profiles. Although other methods show slightly larger deviations, the RMSD values are within about 6% of total adsorption.

The original target set by ARPA-E for CH_4 storage states that, at 298 K and 35 bar, the volumetric storage capacity should exceed 180 v/v for qualified nanoporous materials. Under such conditions, the adsorbed natural gas will have an energy density comparable to that of the compressed natural

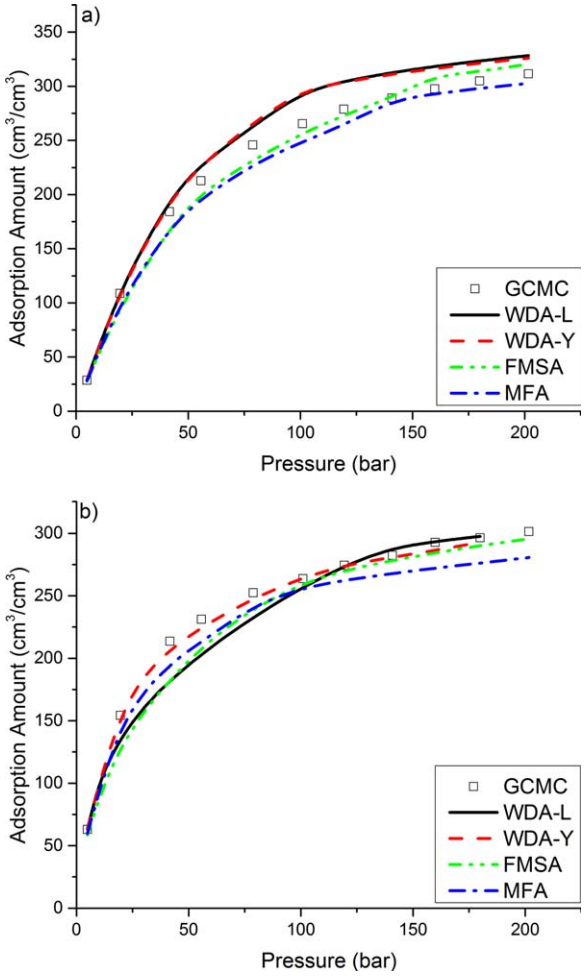

Figure 3. Methane adsorption isotherms at 298K for (a) MOF-5 and (b) Cu-BTC framework materials calculated from GCMC simulation and from different classical DFT methods.

[Color figure can be viewed in the online issue, which is available at wileyonlinelibrary.com.]

gas (CNG) at the same temperature and 250 bar.[11] While that target can be easily reached by many MOF candidates, none of the existing materials meet the new ARPA-E target for methane storage in transportation vehicles.[39] The new ARPA-E target specifies not only the total gas uptake but also the delivery amount by nanoporous materials between compression at 35 bar and release at 5 bar at room temperature. In Figure 4b, we compare methane delivery predicted by MFA and GCMC methods. In general, the MFA predictions agree very well with the simulation data, especially for medium and high loading MOF materials. The deviation becomes more noticeable for materials with high total adsorption but low delivery. Considering the accuracy of MFA prediction for the total methane storage capacity at 298 K and 5 bar (Figure 4a), the large discrepancy for delivery may be attributed to numerical issues in our classical DFT calculations. Because those MOFs have large adsorption capabilities at both 35 and 5 bar, delivery is small and sensitive to numerical details.

Diffusivity

Classical DFT gives the density profile of gas molecules in a porous material that reflects the microscopic details of adsorbent-adsorbate interactions. Not only is the density profile related to the adsorption isotherm, it can also be used to identify important adsorbent-adsorbate interactions and predict other thermodynamic properties including enthalpy of adsorption and excess entropy. While the enthalpy of adsorption is important for practical applications, the excess entropy provides a convenient starting point for predicting transport coefficients over a broad range of thermodynamic conditions.

In our previous work,[28] we have demonstrated that Rosenfeld's excess-entropy scaling method can be combined with the Knudsen model to predict the self-diffusivity of gas molecules in various nanoporous materials. Because the excess entropy is readily available from adsorption calculations and the Knudsen model applies to gas diffusion at infinite dilution, the new computational procedure is much faster than

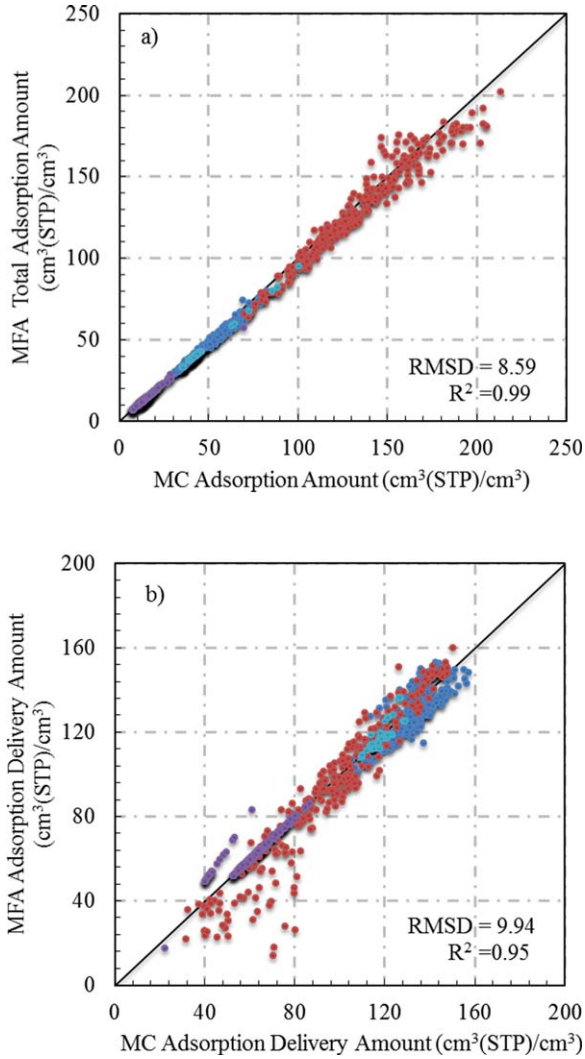

Figure 4. Comparison of methane adsorption at 298 K in 1200 MOFs calculated from GCMC and from MFA methods.

a) Total adsorption amount at 5 bar; b) Delivery amount between 35 bar and 5 bar. Color code: Navy blue, top 300 from excess CH_4 adsorption in weight category; Red, top 300 from excess CH_4 adsorption in volume category; Purple, top 300 from void fraction category; Sky blue, top 300 from surface area (m^2/cm^3) category from the Northwestern Hypothetical MOF Database. [Color figure can be viewed in the online issue, which is available at wileyonlinelibrary.com.]

Table 1. RMSD and Correlation Coefficients (R-value) for Various Classical DFT Methods in Comparison with GCMC Simulation Data for Methane Adsorption in 1200 MOFs at 298 K and 35 bar

	FMSA	MFA	WDA-Y	WDA-L
RMSD cm^3 (STP)/cm^3	16.45	7.90	15.76	16.58
R^2	0.94	0.99	0.98	0.97

traditional MD simulation methods for calculating the gas self-diffusivity over a broad range of thermodynamic conditions.

Figure 5 presents the self-diffusion coefficients of CH_4 in the two MOF materials considered above, MOF-5 and Cu-BTC, at 298 K over a broad range of pressures. The theoretical results are calculated according to Eq. 10. With α treated as an adjustable parameter ($\alpha = 0.42$), the extended excess entropy scaling method is able to reproduce the simulation data almost quantitatively. Semiquantitative results are attainable with approximation $\alpha \approx \alpha_{FCC}$.

Figure 6 shows the self-diffusivities of CH_4 in the top five MOFs that, as identified below, show the highest volumetric delivery (see Table 2). Here, temperature is fixed at 298 K, and α is an adjustable parameter for each material. Again, the extended excess entropy scaling method reproduces the simulation data very well over the entire range of pressures; the approximation $\alpha \approx \alpha_{FCC}$ leads to semiquantitative agreement between theory and MD simulation data. Interestingly, the MOF materials with top delivery show similar gas diffusivity at both low and high loadings, even though their relative ranks are slightly different.

Characteristics of "good" adsorbents

Conventional thermodynamic models for gas adsorption such as Langmuir and BET isotherms presume that, at a given bulk condition, the total gas uptake is linearly proportional to available adsorbent surface area (or accessible surface area). Whereas ambiguity might arise in its definition (or measurement) for a particular porous material, the surface area has been routinely used as an important measure for identification of promising MOFs with large adsorption capability. The significance of surface area has been rarely challenged even after widespread applications of simulation methods.

To find possible correlations between gas adsorption capability and materials surface area, we plot methane adsorption vs. accessible surface area[40,41] for 1200 MOFs materials at 298 K and 35 bar. While Figure 7a shows some positive correlation for total adsorption, no trend in Figure 7b correlates the accessible surface areas and delivery. More important, if one focuses on the top MOF candidates for methane storage (see Figure 8), neither the simulation results nor the classical DFT predictions exhibit any convincing relationship between those two quantities. The decoupling of delivery from the (accessible) surface area is somewhat anticipated because although the geometric accessible surface areas are calculated based on the locus of the surface potential minimum, it only accounts for one gas molecule at a time. The surface area does not take into consideration the correlation between adsorbed gas molecules that is important, especially for candidates with high loading capacities. Conversely, the BET surface area is nicely correlated with adsorption because it is obtained from fitting to the

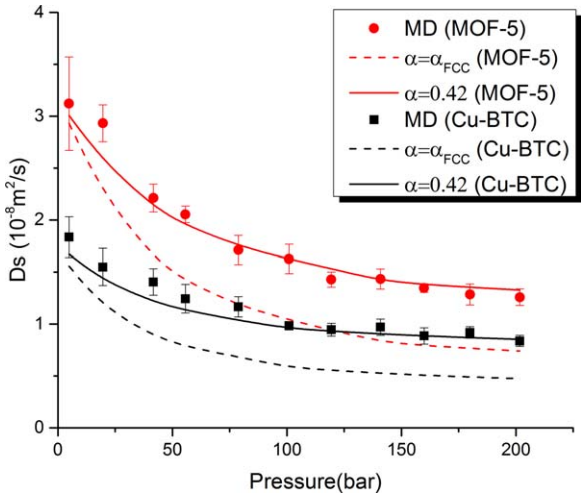

Figure 5. Self-diffusivities of CH_4 molecules in MOF-5 and Cu-BTC at 298 K predicted by MD simulation and by the extended excess-entropy scaling method, respectively.

Filled dots are results from MD simulations, while the lines are obtained from the extended excess-entropy scaling method. [Color figure can be viewed in the online issue, which is available at wileyonlinelibrary.com.]

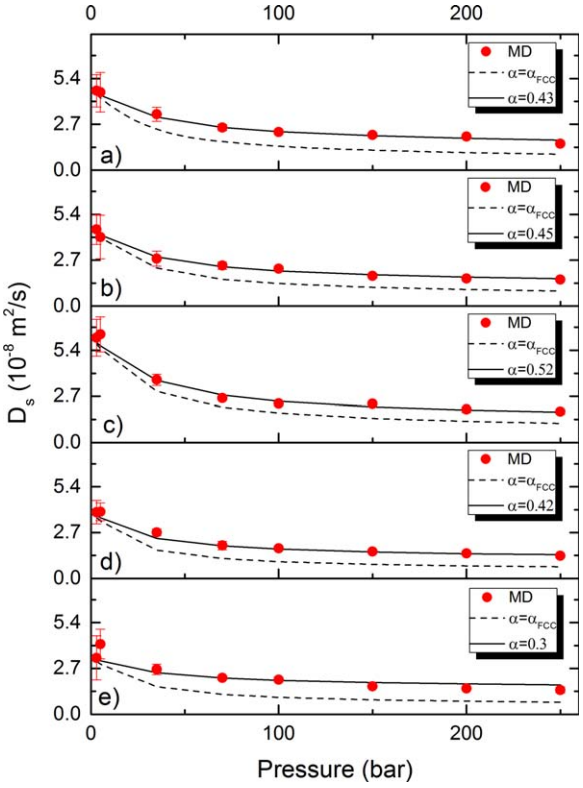

Figure 6. Self-diffusivities of CH_4 in top 5 MOFs with the highest volumetric delivery amount for compression at 233 K and 75 bar and release at 358 K and 5 bar predicted by FMSA method.

The symbols are self-diffusion coefficients predicted by MD simulation, and the lines are from the extended excess-entropy scaling method. [Color figure can be viewed in the online issue, which is available at wileyonlinelibrary.com.]

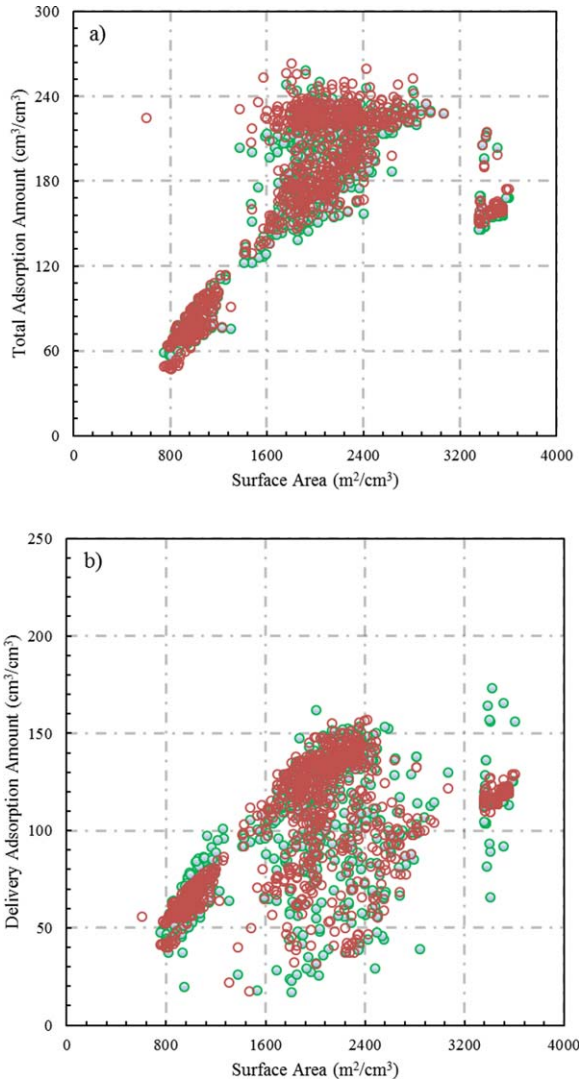

Figure 7. Adsorption of methane in 1200 MOFs at 298 K and 35 bar as a function of the accessible surface area calculated according to the MFA and GCMC methods.

a) Total adsorption amount; b) Delivery amount. Green dots: DFT data; Red dots: GCMC data. [Color figure can be viewed in the online issue, which is available at wileyonlinelibrary.com.]

gas adsorption data. Therefore, good correlation between BET surface area and adsorption capability is not surprising.

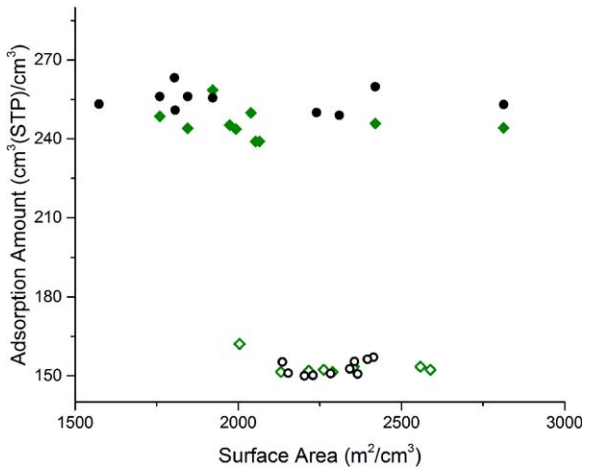

Figure 8. Top 10 MOF candidates with the highest adsorption amounts of methane at 298 K and 35 bar as a function of the accessible surface area.

Cycles: predicted by GCMC; Diamonds: predicted by MFA, while filled ones stand for total adsorption amounts and blank ones for delivery amounts between 298 K, 35 bar and 298 K, 5 bar. [Color figure can be viewed in the online issue, which is available at wileyonlinelibrary.com.]

According to Figure 4 and Supporting Information Figure S1, a material with high methane adsorption capacity does not warrant a large delivery at the ARPA-E conditions. While adsorption capacity appears to be in good correlation with the void fraction, such correlation does not exist for the top candidates. Conversely, Figure 4b shows that MOFs with high CH_4 weight adsorption coincide with those with high delivery, suggesting that it may serve as a good indicator to identify promising materials for methane storage.

ARPA-E MOVE target

Methane delivery capacities for all MOF materials considered in this work are below 160 cm^3/cm^3, far below the ARPA-E target 315 cm^3/cm^3. To achieve the desired volumetric delivery, we could either increase the gas uptake at the compressed stage or reduce the remnant amount upon release. Table 3 summarizes the performance of the top 10 MOFs identified from different theoretical methods if we set the initial pressure to 250 bar, the same as that in a CNG tank. According to this table, the top materials identified by GCMC are in good agreement with those from various classical DFT

Table 2. Top 10 MOF Candidates Identified by GCMC and by Various Classical DFT Methods According to the Volumetric Delivery Amount between Compression at $T = 233$ K, $P = 75$ bar and Release at $T = 358$ K, $P = 5$ bar. As explained in Table 3 $\Gamma_{del,V}$ is given in the units of cm^3(STP)/cm^3 and $\Gamma_{del,M}$ in the units of g/g.

	FMSA			MFA			WDA-Y			GCMC		
Rank	No.	$\Gamma_{del,V}$	$\Gamma_{del,M}$	No.	$\Gamma_{del,V}$	$\Gamma_{del,M}$	No.	$\Gamma_{del,V}$	$\Gamma_{del,M}$	No.	$\Gamma_{del,V}$	$\Gamma_{del,M}$
1	1031	321.4	0.63	1033	315.5	0.53	1111	353.9	0.69	1162	336.1	0.66
2	1037	318.7	0.59	1011	315.2	0.49	1025	352.1	0.68	1026	335.8	0.53
3	1111	318.4	0.62	1022	314.4	0.50	1064	349.2	0.65	1011	335.5	0.52
4	1002	318.2	0.55	1026	313.9	0.49	1034	348.9	0.68	1007	335.3	0.59
5	1007	318.2	0.56	1013	312.7	0.50	1041	348.2	0.68	1145	335.3	0.68
6	1055	318.1	0.57	1046	312.2	0.45	1030	347.9	0.67	1031	334.7	0.65
7	1025	317.7	0.61	1098	311.7	0.47	1055	346.0	0.62	1019	334.6	0.51
8	1033	317.6	0.53	1044	311.7	0.46	1071	345.9	0.60	1001	334.2	0.58
9	1010	317.5	0.55	1019	311.0	0.47	1086	345.8	0.70	1071	334.1	0.58
10	1011	317.3	0.49	1197	310.5	0.48	1033	345.1	0.57	1087	333.9	0.59

Table 3. Top 10 MOF Candidates Identified by GCMC and by Various Classical DFT Methods According to the Volumetric Delivery Amount: the Methane Delivery Amount is Calculated between Compression at $T = 298$ K, $P = 250$ bar and Release at $T = 298$ K, $P = 5$ bar.

	FMSA			MFA			WDA-Y[b]			GCMC		
Rank	No.	$\Gamma_{del,V}$	$\Gamma_{del,M}$	No.	$\Gamma_{del,V}$	$\Gamma_{del,M}$	No.	$\Gamma_{del,V}$	$\Gamma_{del,M}$	No.	$\Gamma_{del,V}$	$\Gamma_{del,M}$
1	1101	300.5	0.63	1033	272.1	0.45	1213	307.4	0.66	1031	290.1	0.57
2	1089	299.1	0.62	1101	271.8	0.57	1101	306.7	0.64	1089	290.1	0.60
3	1213	298.7	0.64	1031	271.6	0.53	1089	305.2	0.64	1101	290.0	0.61
4	1031	297.5	0.58	1213	271.1	0.58	1031	304.1	0.59	1213	289.8	0.62
5	1111	295.7	0.58	1089	270.9	0.56	1111	303.2	0.59	1111	287.1	0.56
6	1052	295.6	0.60	1026	269.7	0.42	1025	301.9	0.58	1034	287.0	0.56
7	1145	295.2	0.60	1111	269.5	0.53	1145	301.8	0.61	1086	286.8	0.58
8	1025	294.5	0.57	1064	268.7	0.50	1052	300.6	0.61	1030	286.5	0.55
9	1086	294.2	0.59	1025	268.7	0.52	1233	300.4	0.73	1145	286.5	0.58
10	1034	294.1	0.57	1052	268.6	0.54	1086	299.9	0.60	1052	286.2	0.58

[a]The No. represents the serial number in the Northwestern Hypothetical MOF Database, while the 1st digit means the category (1 for excess CH_4 adsorption in weight category; 2 for excess CH_4 adsorption in volume category; 3 for void fraction category; 4 for surface area (m^2/cm^3) category), the last 3 digits means the rank in the category. Γ_{del} means delivery amount, where V stands for adsorption amount in units of cm^3(STP)/cm^3 and M stands for adsorption amount in units of g/g. (http://hmofs.northwestern.edu/hc/crystals.php)
[b]Since the two WDA methods give nearly the same results, here we give only the WDA-Y data.

methods. For the top candidates, the list of MOFs generated from FMSA agrees the best with that from simulation, with 9 out of 10 materials identical.

If the initial compression pressure is set to 250 bar, many MOFs may meet the target for weight delivery of 0.5 g/g, and the best material is able to achieve up to 95% of the volumetric ARPA-E target. If we raise the release temperature to 358 K, the ARPA-E volumetric target may also be reached (see Supporting Information Table S1). Alternatively, the ARPA-E target can be reached by reducing the initial storage temperature to 233 K, the lowest operation temperature according to DOE instructions. In that case, many MOFs could reach the ARPA-E target by compression at 75 bar and release at 298 K and 5 bar (see Supporting Information Table S2). At higher release temperature, all top 10 MOFs achieve the ARPA-E methane storage target for both gravimetric and volumetric targets (see Table 3).

Unlike the results shown in Table 1, the classical DFT and GCMC methods predict different top 10 candidates to meet the ARPA-E target (see Table 3). Nevertheless, all these materials exhibit similar adsorption capabilities. The GCMC candidates are among the top 50 materials identified by the classical DFT methods. In both Tables 1 and 3, there are about 3% numerical discrepancies between DFT and GCMC data. Considering 5% statistical error in typical GCMC simulations, we believe the classical DFT methods should be sufficiently accurate to identify promising MOF materials for further experimental investigations.

Conclusions

We have calibrated four versions of classical DFT for potential applications to the discovery of novel MOFs for methane storage. Overall, the classical DFT methods show good agreement with the simulation results for methane adsorption in slit pores as well as in MOF-5 and Cu-BTC. Their relative performance is sensitive to thermodynamic conditions and depends also on the specific material under consideration. Using the ARPA-E methane delivery capabilities of over 1200 MOFs as the benchmark, we find that, surprisingly, the results from the MFA agree best with the simulations data, with a RMSD of only 7.90 cm^3(STP)/cm^3. Considering its theoretical simplicity, we conclude that MFA is probably the best choice for screening nanostructured materials for methane storage. While this work focuses on methane adsorption and shows that classical DFT is a promising computational tool for materials screening, a similar conclusion holds for adsorption of other gases including those with partial atomic charges, provided that an accurate Helmholtz energy functional is available. Working along this direction is under current investigation and will be reported in future publications.

Whereas the BET surface area is conventionally used as a benchmark to identify nanoporous materials with large adsorption capacity, we find that, in general, there is no convincing correlation between a geometric surface area and the net delivery at conditions relevant to methane storage. While none of the existing materials satisfies the ARPA-E target, many MOFs can be identified to give a weight delivery exceeding 0.5 g/g if the initial compression pressure is modified to 250 bar, the same as that in a CNG tank. The volumetric target may also be reached if the release temperature is raised to 358 K. Alternatively, the ARPA-E target can be fulfilled by reducing the initial storage temperature to 233 K, the lowest operation temperature according to DOE instruction.

The classical DFT is computationally extremely efficient when compared with conventional simulation methods, in particular for calculating thermodynamic properties for a large library of materials over a broad parameter space. Figure 9 shows the statistics of the computational time for

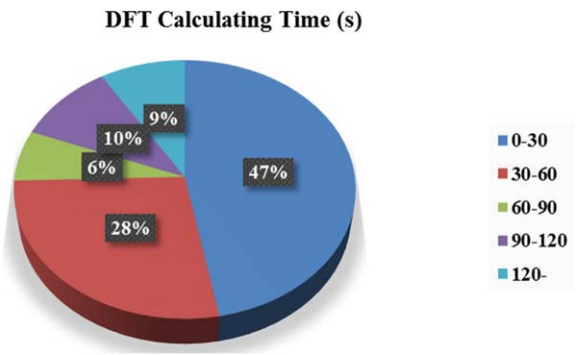

Figure 9. Distribution of computational time for predicting methane adsorption in 1200 MOFs with MFA.

[Color figure can be viewed in the online issue, which is available at wileyonlinelibrary.com.]

implementing classical DFT calculations on a single desktop computer (i.e., one 3.0 GHz Sandy Bridge CPU core). The average computational time is within 2 min for each sample, which is faster than that for conventional GCMC simulation by more than one order of magnitude. DFT provides quantitative information on the excess entropy that can be used for predicting gas self-diffusivities in porous materials, important for practical applications but extremely time-consuming to calculate using conventional simulation methods. Good performance and computational efficiency make classical DFT a suitable choice for high-throughput calculations.

Acknowledgment

For financial support of this research, the authors are grateful to the U. S. Department of Energy (DE-FG02-06ER46296).

Literature Cited

1. Yang RT. *Gas Separation by Adsorption Processes*. Singapore; River Edge, NJ: World Scientific, 1997.
2. Duong DD. *Adsorption analysis: equilibria and kinetics*. London: Imperial College Press, 1998.
3. Myers AL, Prausnitz JM. Thermodynamics of mixed-gas adsorption. *AIChE J*. 1965;11:121–127.
4. Myers AL, Monson PA. Physical adsorption of gases: the case for absolute adsorption as the basis for thermodynamic analysis. *Adsorption*. 2014;20:591–622.
5. Snurr RQ. New horizons for the physical chemistry of nanoporous materials. *J Phys Chem Lett*. 2011;2:1842–1843.
6. Ockwig NW, Delgado-Friedrichs O, O'Keeffe M, Yaghi OM. Reticular chemistry: occurrence and taxonomy of nets and grammar for the design of frameworks. *Acc Chem Res*. 2005;38:176–182.
7. Keskin S, Liu J, Rankin RB, Johnson JK, Sholl DS. Progress, opportunities, and challenges for applying atomically detailed modeling to molecular adsorption and transport in metal-organic framework materials. *Ind Eng Chem Res*. 2009;48:2355–2371.
8. Jiang JW, Babarao R, Hu ZQ. Molecular simulations for energy, environmental and pharmaceutical applications of nanoporous materials: from zeolites, metal-organic frameworks to protein crystals. *Chem Soc Rev*. 2011;40:3599–3612.
9. Yang QY, Liu DH, Zhong CL, Li JR. Development of computational methodologies for metal-organic frameworks and their application in gas separations. *Chem Rev*. 2013;113:8261–8323.
10. Getman RB, Bae YS, Wilmer CE, Snurr RQ. Review and analysis of molecular simulations of methane, hydrogen, and acetylene storage in metal-organic frameworks. *Chem Rev*. 2012;112:703–723.
11. Wilmer CE, Leaf M, Lee CY, Farha OK, Hauser BG, Hupp JT, Snurr RQ. Large-scale screening of hypothetical metal-organic frameworks. *Nat Chem*. 2012;4:83–89.
12. Colon YJ, Snurr RQ. High-throughput computational screening of metal-organic frameworks. *Chem Soc Rev*. 2014;43:5735–5749.
13. Wu D, Wang CC, Liu B, Liu DH, Yang QY, Zhong CL. Large-scale computational screening of metal-organic frameworks for CH_4/H_2 separation. *AIChE J*. 2012;58:2078–2084.
14. Sun WZ, Lin LC, Peng X, Smit B. Computational screening of porous metal-organic frameworks and zeolites for the removal of SO_2 and NO_x from flue gases. *AIChE J*. 2014;60:2314–2323.
15. Tadmor EB, Miller RE. *Modeling materials: continuum, atomistic, and multiscale techniques*. Cambridge; New York: Cambridge University Press, 2011.
16. Hohenberg P, Kohn W. Inhomogeneous electron gas. *Phys Rev B*. 1964;136:864–871.
17. Evans R. Nature of the liquid-vapor interface and other topics in the statistical-mechanics of nonuniform, classical fluids. *Adv Phys*. 1979; 28:143–200.
18. Parr RG, Yang W. *Density-functional theory of atoms and molecules*. New York: Oxford University Press, 1989.
19. Wu JZ. Density functional theory for chemical engineering: from capillarity to soft materials. *AIChE J*. 2006;52:1169–1193.
20. Lastoskie C, Gubbins KE, Quirke N. Pore size distribution analysis of microporous carbons: a density functional theory approach. *J Phys Chem*. 1993;97:4786–4796.
21. Fu J, Liu Y, Wu JZ. Molecular density functional theory for multiscale modeling of hydration free energy. *Chem Eng Sci*. 2015;126: 370–382.
22. Fu J, Liu Y, Tian Y, Wu JZ. Density functional methods for fast screening of metal-organic frameworks for hydrogen storage. *J Phys Chem C*. 2015;119:5374–5385.
23. Tang YP, Wu JZ. Modeling inhomogeneous van der Waals fluids using an analytical direct correlation function. *Phys Rev E*. 2004;70: 011201–011208.
24. Ravikovitch PI, Neimark AV. Density functional theory model of adsorption on amorphous and microporous silica materials. *Langmuir*. 2006;22:11171–11179.
25. Yu Y-X. A novel weighted density functional theory for adsorption, fluid-solid interfacial tension, and disjoining properties of simple liquid films on planar solid surfaces. *J Chem Phys*. 2009;131:024704–024715.
26. Liu Y, Liu HL, Hu Y, Jiang JW. Development of a density functional theory in three-dimensional nanoconfined space: H_2 storage in metal-organic frameworks. *J Phys Chem B*. 2009;113:12326–12331.
27. Yu Y-X, Wu J. Structures of hard-sphere fluids from a modified fundamental-measure theory. *J Chem Phys*. 2002;117:10156–10164.
28. Liu Y, Fu J, Wu J. Excess-entropy scaling for gas diffusivity in nanoporous materials. *Langmuir*. 2013;29:12997–13002.
29. Martin MG, Siepmann JI. Transferable potentials for phase equilibria. 1. united-atom description of n-alkanes. *J Phys Chem B*. 1998; 102:2569–2577.
30. Rappe AK, Casewit CJ, Colwell KS, Goddard WA, Skiff WM. Uff, a full periodic-table force-field for molecular mechanics and molecular-dynamics simulations. *J Am Chem Soc*. 1992;114:10024–10035.
31. Wu JZ. *Density functional theory for liquid structure and thermodynamics In: Molecular thermodynamics of complex systems*. Berlin: Springer, 2009:1–74.
32. Johnson JK, John AZ, Gubbins KE. The Lennard-Jones equation of state revisited. *Mol Phys* 1992;78:591–618.
33. Tang YP, Wu JZ. A density-functional theory for bulk and inhomogeneous Lennard-Jones fluids from the energy route. *J Chem Phys*. 2003;119:7388–7397.
34. He P, Liu H, Zhu J. Tests of excess entropy scaling laws for diffusion of methane in silica nanopores. *Chem Phys Lett*. 2012;535:84–90.
35. Rosenfeld Y. Relation between transport coefficients and internal entropy of simple systems. *Phys Rev A*. 1977;15:2545–2549.
36. Eddaoudi M, Kim J, Rosi N, Vodak D, Wachter J, O'Keeffe M, Yaghi OM. Systematic design of pore size and functionality in isoreticular MOFs and their application in methane storage. *Science*. 2002;295:469–472.
37. Chui SSY, Lo SMF, Charmant JPH, Orpen AG, Williams ID. A chemically functionalizable nanoporous material $[Cu_3(TMA)_2(H_2O)_3]_n$. *Science*. 1999;283:1148–1150.
38. Addicoat MA, Coupry DE, Heine T. AuToGraFS: automatic topological generator for framework structures. *J Phys Chem A*. 2014; 118:9607–9614.
39. Methane Opportunities for Vehicular Energy. Available at: http://arpa-e.energy.gov/?q=arpa-e-programs/move. Accessed on November, 2014.
40. Walton KS, Snurr RQ. Applicability of the bet method for determining surface areas of microporous metal−organic frameworks. *J Am Chem Soc*. 2007;129:8552–8556.
41. Sarkisov L, Harrison A. Computational structure characterisation tools in application to ordered and disordered porous materials. *Mol Sim*. 2011;37:1248–1257.

Manuscript received Dec. 9, 2014, and revision received Apr. 29, 2015.